Quantitative measurement of temperature in oxygen enriched $CH_4/O_2/N_2$ premixed flames using Laser Induced Thermal Grating Spectroscopy (LITGS) up to 1.0 MPa

Akihiro Hayakawa[1], Tomohisa Yamagami[1], Kiyonori Takeuchi[1], Yasuhiro Higuchi[1], Taku Kudo[1], Steven Lowe[2], Yi Gao[3], Simone Hochgreb[2], Hideaki Kobayashi[1]

1 *Institute of Fluid Science, Tohoku University, Japan*
2 *Department of Engineering, University of Cambridge, United Kingdom*
3 *School of Mechanical Engineering, Shanghai Jiao Tong University, China*

Corresponding author
Akihiro Hayakawa
Institute of Fluid Science, Tohoku University
2-1-1 Katahira, Aoba-ku, Sendai, Miyagi 980-8577, Japan
Tel. +81-22-217-5273
Fax. +81-22-217-5323
E-mail hayakawa@flame.ifs.tohoku.ac.jp

Colloquium
Diagnostics

Total length of paper
6162

Listing of the word equivalent length

Abstract	186	
Main text	3812	
Equations	147	
Nomenclature	0	
References	455	
Figures (total)	1748	
Table (total)	0	6162

Number of words of main text was counted by MS-Word (Method 1)

Equivalent length with caption	Fig. No. (length)
Figure	1 (348), 2 (235), 3 (117), 4 (305), 5 (475), 6 (130), 7 (138)

No color images to be charged are included.

Abstract

The application of laser diagnostics to high pressure combustion phenomena is particularly challenging, especially in practical combustors such as rocket motors. In this study, temperature measurements using Laser Induced Thermal Grating Spectroscopy (LITGS) are demonstrated in oxygen enriched $CH_4/O_2/N_2$ premixed laminar flames at pressures up to 1.0 MPa. We use a previously developed OH absorption LITGS technique to determine product gas temperatures from 0.3 to 1.0 MPa, for both high temperature oxygen-enriched and pure-oxygen flames, for measurements up to 3000 K. Further, we demonstrate how it is necessary to correct the measurements for the local absorption of laser light to obtain accurate temperatures, and offer a technique for producing the correction by using different laser energies. Once the correction is applied, we demonstrate that the measurements at 0.5 MPa are within 1.6% of the adiabatic non-strained flame temperatures, with a standard deviation of about 160 K, thus offering a competitive method for the challenging conditions at high pressures and temperatures. The values obtained at derived temperatures at 1.0 MPa were slightly lower than the adiabatic unstrained flame temperatures, which could possibly be attributed to heat losses.

Keywords

LITGS; High temperature; High pressure; Quantitative temperature measurement; Oxygen enriched flames

1. Introduction

Many combustors in devices such as reciprocating engines, gas turbine and rocket motors operate at high pressures in order to increase power density. This is particularly true in the case of rocket motors, where hydrogen-oxygen combustion at pressures of order 10 MPa [1] is employed and temperatures are expected to be in excess of 3000 K. Yet these extreme pressures and temperatures render the measurement of scalar quantities particularly challenging, as optical techniques can be limited by light absorption and spectral broadening [2].

Temperature is a key controlling scalar in most combustion systems, so that there is an extensive research effort to produce quantitative measurements of flame temperatures. These tools include the use of thermocouples (e.g. [3]), Rayleigh scattering (e.g. [4]), Coherent anti-Stokes Raman spectroscopy (CARS) (e.g. [5]), Laser Induced Electrostrictive Gratings (LIEGS) (e.g. [6]), and Laser Induced Thermal Grating Spectroscopy (LITGS) [7-19]. The high pressures prevalent in gas turbines and rocket systems create significant challenges for optical diagnostics. Whereas on one hand, the higher concentrations help produce higher signal from the larger number of molecules per unit volume interacting with light, countervailing effects can reduce the signal to noise ratio of the techniques, including: (a) background radiant interference from intense chemiluminescence, which interferes with spectroscopic diagnostics such as fluorescence or Rayleigh scattering, (b) line broadening from techniques which rely on a well-defined spectrum, such as Planar Laser Induced Fluorescence (PLIF), and (c) increased signal trapping and quenching from collisions, particularly in the case of fluorescence.

In contrast with these techniques, LITGS offers potential advantages for quantitative measurements of temperature at high pressure. Unlike many other laser-based techniques, the signal and signal/noise ratio produced increases with pressure. As detailed further on, this is because the signal intensity is proportional to the square of the induced refractive index fluctuation [15], which increases with the density of the mixture. A number of studies using LITGS have been used in non-reacting [8-13] and reacting [14-19] flows. Although LITGS can only be used in the presence of an absorbing species, LITGS also offers the advantage of significantly higher signal relative to LIEGS,

and less stringent requirements on optical alignment relative to CARS.

Despite the growing interest associated with LITGS measurements, only a handful of studies have used LITGS for measuring product gas temperatures. The reasons are: low concentration of species to be excited in the product gas especially at low pressure; an immediate decay of signal due to high thermal diffusivity at low pressures. Absorption by the hydroxyl radical OH around 307 nm was used in measurements of product temperature over a flat-flame burner stabilized using H_2/O_2 at atmospheric pressures [14], and CH_4/air mixtures at pressures from 1.0 to 4.0 MPa [16]. More recently, Sahlberg *et al*. [18] obtained LITGS signals over an atmospheric pressure ethylene flame using infrared absorption around 3.2 μm for both the fuel itself and H_2O to generate the thermal grating. Since fuel in unburnt mixture and water vapor in product gas are major components, a stronger LITGS signal than for OH is expected even at low pressure.

A comparison of the expected OH concentrations in the experiments by Latzel *et al*. [16] with those in oxygen-enriched, high temperature flames suggested that the latter might be as high or higher than in the original experiments, thus allowing higher quality measurements. Therefore, the purpose of this study is to demonstrate the capability of LITGS using OH excitation for product gas temperature measurements in high pressure and high temperature, oxygen-enriched flames.

2. Temperature measurement using OH-LITGS

2.1. Theory of LITGS

The LITGS technique has been described in detail elsewhere (see [7]), so the following description is limited to the basic theory. In LITGS, pulsed pump laser beams at a wavelength, λ, cross at an angle $2\theta_p$ at a probe volume, generating a grating of spacing $\Lambda = \lambda/(2\sin\theta_p)$. The pump wavelength targets a specific transition for molecular excitation of a particular species of interest, so that the molecules in the regions of high intensity within the grating absorb energy during the short (nanoseconds) laser pulse. Part of the energy absorbed is released via collisional quenching in the form of thermal energy, generating a stationary temperature and density perturbation, in the form of a

thermal grating across the interacting region, which decays due to the thermal diffusion over hundreds of nanoseconds. The rapid temperature change generates an acoustic wave which propagates locally through the thermal grating. The interference of traveling acoustic and stationary density perturbations creates a local density oscillation. The latter is probed by using a continuous wave laser beam of a different wavelength, λ_p, directed at the Bragg angle, $\theta_b = \sin^{-1}[\lambda_p/(2\Lambda)]$. Bragg diffraction off the grating generates a coherent signal beam which, when collected, yields the local temporal evolution of the overall density oscillation.

The frequency of the LITGS signal oscillation, f_{osc}, is equal to the inverse time required for the passage of the sound wave through the grating spacing Λ at a velocity, a,

$$f_{osc} = \frac{a}{\Lambda}. \tag{1}$$

The speed of sound in an ideal gas is given by:

$$a = \sqrt{\frac{\gamma R^* T}{W}}, \tag{2}$$

where γ, R^*, W and T are the specific heat ratio, the universal gas constant, mean molecular weight and temperature, respectively. From Eqs. (1) and (2), the temperature within the probe volume can finally be determined as:

$$T = \frac{W}{\gamma R^*} \Lambda^2 {f_{osc}}^2. \tag{3}$$

2.2. Experimental setup and experimental conditions

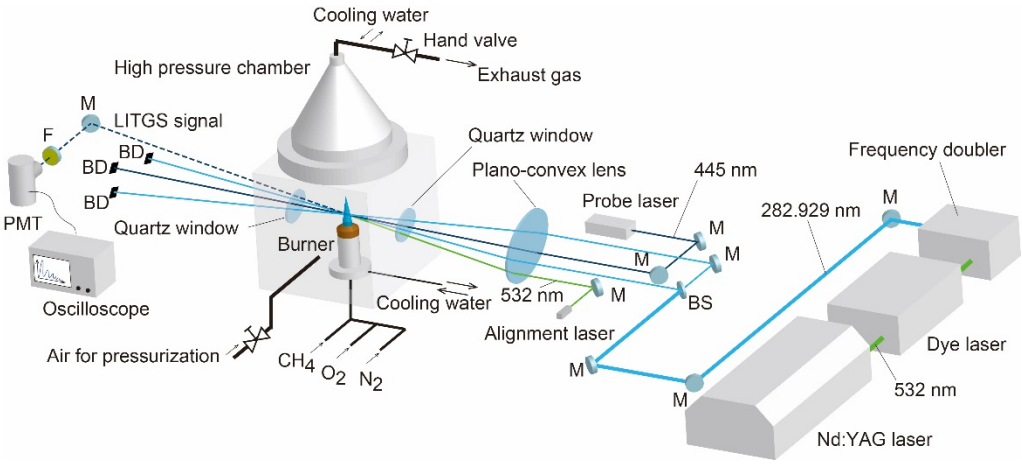

Figure 1. Experimental setup and the layout of the optical geometry through the high pressure chamber for high pressure OH-LITGS experiments. The symbols M, BS, BD, F and PMT represent mirror, beam splitter, beam dump, interference filter and photo multiplier tube, respectively.

Figure 1 shows the experimental setup and the layout of the optical geometry through the high pressure combustion chamber. The high pressure combustion experiments were carried out using the combustion test facility at the Institute of Fluid Science, Tohoku University. Details of the test facility have been described elsewhere [20]. A Nd:YAG laser (Spectra-Physics, GCR-250, 532 nm) pumping a frequency doubled dye laser (Lumonics, HD500+HT1000) was employed to obtain a pump beam set to a wavelength of 282.929 nm for the $Q_1(6)$ branch of OH(1,0) band excitation. The pump energy for OH excitation was measured before the beam splitter and set to 9 mJ. The pump beam was split using a 50:50 beam splitter to separate two laser beams, and the parallel beams are introduced via a plano-convex lens (OptoSigma, focal length, F=1000 mm at 546.1 nm), termed as the crossing lens in this paper. The distance between the two pump laser beams, δ, was set to 10 mm. The two beams are crossed at the measurement point with an angle of $2\theta_p$. The refractive index inside the chamber and of the flame changes slightly with changes in the pressure inside the chamber, and so does the optimum alignment. In order to maximize the LITGS signal, the alignment was adjusted before the series of

experiments at the same pressure condition.

A continuous wave (CW) semiconductor laser, operating at a wavelength of 445 nm (RGB laser system, NavoPro PB 445-1000 MM) was employed as the probe beam. The power for the probe beam was set to 810 mW. The beams passing through the high pressure chamber were stopped by beam dumps. The diffracted signal (LITGS signal) was detected using a photo multiplier tube (PMT, Hamamatsu Photonics, R928) through an interference filter (OptoSigma, YIF-BA420-460S) that transmits the beam at 445 nm. The LITGS signal was acquired using an oscilloscope with a sampling rate of 10 GS/s and 500 MHz bandwidth (Keysight, DSOS054A).

The pump beam diameter at the crossing lens was measured at the crossing point and found to be slightly elliptical, with major and minor axes around 4.7 mm and 3.4 mm, respectively. By assuming a Gaussian profile of pump beams, the lengths of the measurement volume in the forward beam axis direction and two perpendicular directions were about $19.0 \times 0.1 \times 0.1$ mm. The relatively long focal length of the crossing lens employed in this study yields a relatively long measurement volume. However, the actual measurement point volume is the intersected volume of the two pump beams and the probe beam, and is thus smaller than that implied by the values above. In this study, measurements were performed at the center of the burner, where the temperature gradients within the measurement volume are expected to be small according to the flame observation by OH-PLIF that will be shown in Section 3.1. Smaller probe volumes could of course be realized by increasing the crossing angle, θ_p, but require a different optical arrangement with a larger crossing lens with a shorter focal length.

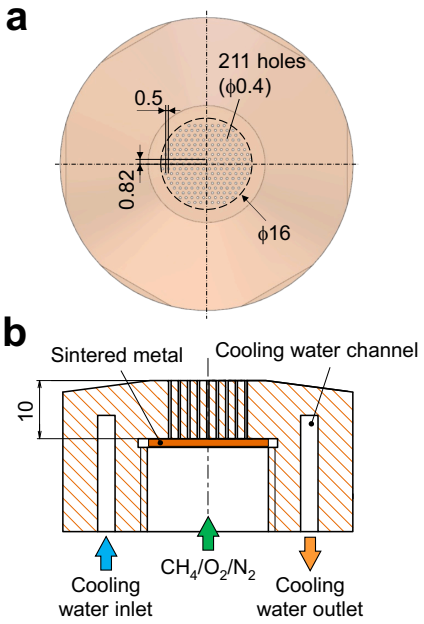

Figure 2. Schematic figures of the modified burner nozzle for the calibration burner developed by Takeuchi et al. [21]: (a) Top-view; (b) Cross-sectional-view.

Oxygen enriched mixtures of CH_4, O_2 and N_2 were considered in this study. The oxygen ratio in the (O_2+N_2) mixture is denoted as, $\beta = Q_{O2}/(Q_{N2}+Q_{O2})$, where Q_x is the volumetric flow rate of species x. The calibration burner available at high pressure developed by Takeuchi *et al.* [21] was employed in this study. A modified burner nozzle which is schematically shown in Fig. 2 was mounted in order to prevent from flashback of oxygen enriched flame. The burner nozzle was made of oxygen-free copper and was water cooled. The nozzle has 211 holes, each with a diameter of 0.4 mm, drilled within a 16 mm circular exit. The measurement points were made at a centerline position located 15 mm downstream of the burner surface. Experiments were performed at pressures, P, of 0.3, 0.5 and 1.0 MPa, and the reactant temperature was 298 K. The equivalence ratio was varied from 0.6 to 1.2 for $CH_4/O_2/N_2$ flames and 0.3 to 0.6 for CH_4/O_2 flames.

3. Results and discussions

3.1. Flame characteristics stabilized on the calibration burner

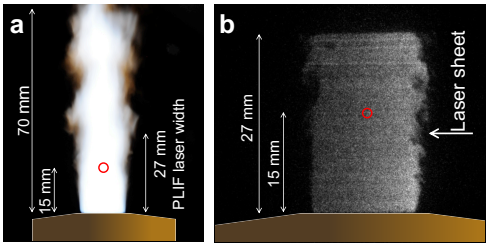

Figure 3. (a) Flame image of direct photo and (b) instantaneous OH-PLIF image at P = 1.0 MPa for ϕ = 1.0 and β = 0.6.

Figure 3 shows the direct photo and OH-PLIF image of a flame stabilized on the calibration burner at P = 1.0 MPa for ϕ = 1.0 and β = 0.6. OH-PLIF images were collected at 263.580 nm excitation for OH(2,0) band excitation [2, 21] in order to reduce the influence of laser attenuation. The laser energy for OH-PLIF was 14 mJ. The circle in Fig. 3 represents the center of the measurement point of LITGS. The broadband white emission in the downstream region of the oxygen-enriched flames could be observed, whereas the interfaces of the hole-stabilized flames on the burner surface were too small to be resolved. The Reynolds numbers based on the hole diameter and mean velocity were about 3000 at 1.0 MPa, and thus somewhat higher than the critical transitional Reynolds number, making the flow weakly turbulent. However, as shown in Fig. 3b, the burned gas downstream the burner was uniform. At other pressure conditions, the Reynolds numbers were smaller than 2300.

Numerical simulations were performed using CHEMKIN-PRO [22] with GRI-Mech 3.0 [23] to determine expected species molar fractions and temperatures. The experimentally measured heat loss to the burner was estimated from the flow rate of water and the inlet and outlet water temperatures. The estimated ratio of heat loss to the burner as a fraction of the heat release was varied from 1.5-9.9%. Adiabatic non-stretched calculations were used as a reference for the numerical simulation, yet the heat loss ratio suggests the calculated values should be considered an upper bound. The maximum expected molar fraction of OH at a height above burner 15 mm downstream of the point of peak heat release rate reaches about 5% for β = 0.6 and 10% for β = 1.0.

The measurements of OH-PLIF confirm that OH fluorescence levels are uniform around the

measurement point [21], although the fluorescence levels decrease strongly from right to left due to laser beam intensity decrease by absorption because of the high OH concentrations at 1.0 MPa.

3.2. Derived temperature from LITGS signal

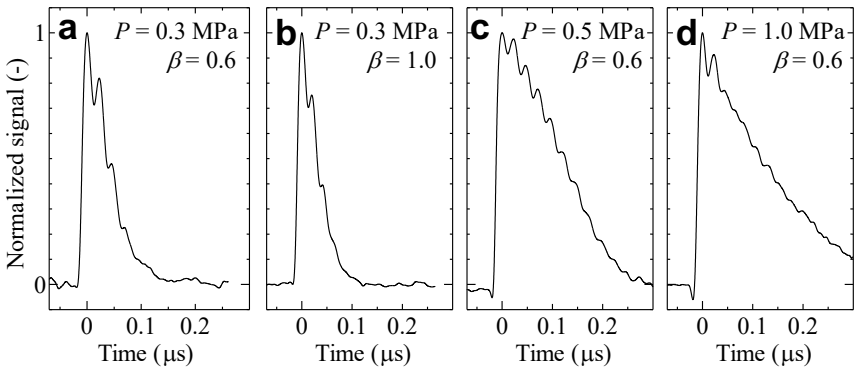

Figure 4. Representative single shot LITGS signal for the equivalence ratio of ϕ = 0.6: (a) P = 0.3 MPa, β = 0.6; (b) P = 0.3 MPa, β = 1.0; (c) P = 0.5 MPa, β = 0.6; (d) P = 1.0 MPa, β = 0.6.

Figure 4 shows single shot LITGS signals. Here, the zero time origin is defined as the instant of the first local peak of the LITGS signal. As mentioned in Section 2.2, the alignment was slightly adjusted before the series of constant pressure conditions, so the LITGS signals could not be exactly directly compared under various pressure conditions. Therefore, the representative signal normalized by the peak value in each case is shown in the figure. The increase in pressure (and density) leads to a slower decay in the LITGS signal, as the thermal diffusivity decreases. Only a few clear peaks were observed (Figs. 4a and 4b) because of significantly fast decay of LITGS signal at 0.3 MPa. The number of local peaks and troughs observed increased at 0.5 MPa (Fig. 4c). However, the contrast between peaks and troughs was poorer for 1.0 MPa than 0.5 MPa. Although this may require further investigation, the high concentration of water vapor inside the high pressure conditions led to condensation on the windows and poorer signal quality (Fig. 4d).

The oscillation frequency, f_{osc}, was determined as the averaged value of the frequency obtained

231 as the inverse of the time between the first two local peaks and troughs rather than a Fourier transform.
232 In some borderline cases, LITGS signals had small and fast decaying oscillation, as shown in Fig. 4b.
233 A total of 512 traces were acquired for all experimental conditions but only the signals that clearly
234 contained two local peaks and troughs were used for the analysis, resulting in a yield of 36 to 511
235 traces used to determine the oscillation frequency, depending on the experimental condition. The mean
236 oscillation frequency and standard deviation were determined from the collected signals. This value
237 was squared, and the temperature evaluated using Eq. (3). Initially, the grating spacing Λ was evaluated
238 based on the distance of two pump beams and the nominal value of focal length of the crossing lens
239 (1000 mm).

240 Equation (3) shows that the estimate of temperature depends on the values of W/γ, which is a
241 function of composition and temperature. In this study, W/γ values were calculated based on the
242 temperature and mixture composition calculated using the CHEMKIN simulation at 15 mm
243 downstream from the position of maximum heat release rate in unstrained, adiabatic free flame
244 simulations. As discussed in Section 3.1, heat loss is not entirely negligible, yet the sensitivity of the
245 values of W/γ to heat loss is small. A decrease in the assumed temperature by a maximum of 10.2%,
246 corresponding to the maximum heat loss, leads to a change in W/γ of 6.7% at the condition of P = 0.5
247 MPa, β = 0.6 and ϕ = 1.0. A change in the equivalence ratio of reactants by 1% leads to a change in γ
248 and W of less than 0.5%.
249

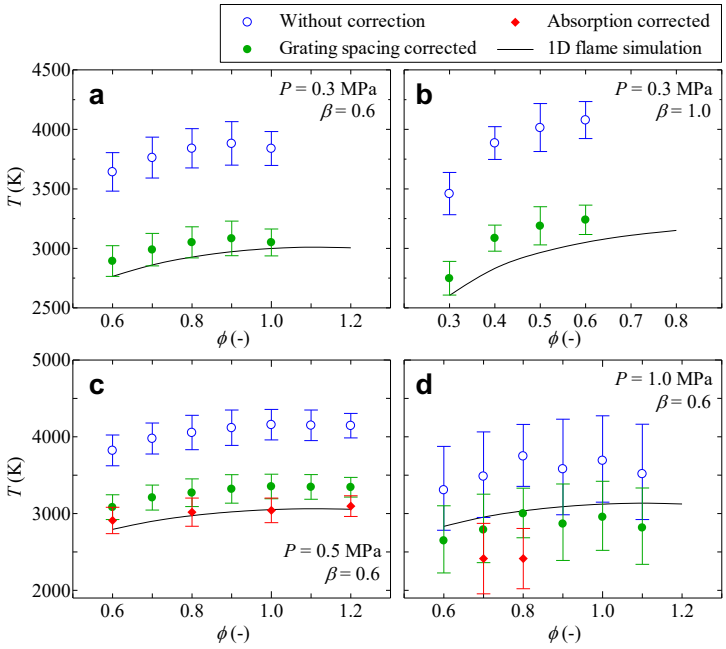

Figure 5. Derived temperature from the LITGS signals with and without corrections (see text): (a) P = 0.3 MPa, β = 0.6; (b) P = 0.3 MPa, β = 1.0; (c) P = 0.5 MPa, β = 0.6; (d) P = 1.0 MPa, β = 0.6. Solid lines are obtained from unstrained flame simulations.

The open circle symbols in Fig. 5 shows the derived LITGS temperature as a function of equivalence ratio and oxygen ratio. As mentioned above, the signal to noise ratio at 1.0 MPa was relatively small compared to other pressure conditions. Therefore, the error bars of the derived temperature were relatively wider and larger than the results by Latzel *et al.* [16] because of the influence on high concentration of water vapor inside the chamber and the small amount of water vapor condensed on the windows. Clearly, the measured LITGS temperature were 500 - 1000 K higher than the temperature calculated from CHEMKIN simulations. Whereas lower temperatures might have been justified from heat loss calculations, higher temperatures can hardly be justified, and the reason for the discrepancy must lie elsewhere.

4. Temperature correction

4.1. Grating spacing correction

The temperatures derived from Eq. (3), depend on the accuracy of the determination of the

properties of the mixture (γ and W), grating spacing, Λ, and oscillation frequency, f_{osc}. The value of grating spacing is particularly important because the derived temperature is proportional to the square of grating spacing as shown in Eq. (3).

In the original analysis, the grating spacing, Λ, was determined by the geometric incident angle, which is a function of the pump beam separation and the focal length of the crossing lens. The focal length of the crossing lens used in this study was specified at a wavelength of 546.1 nm, and the actual focal length was therefore about 10% shorter than the nominal value because of chromatic aberration, resulting in an originally estimated grating spacing of 28.3 μm. In order to obtain a more precise estimate, an atmospheric pressure measurement of temperature using acetone vapor/air non-reacting mixture was done for calibration purposes [19, 24]. Acetone vapor was generated by a gas bubbler, and diluted using dry air down to a value known not to affect the local temperature measurements by local absorption, as discussed in Section 4.2. The local temperature at the outlet of the nozzle for acetone vapor/air mixture was measured by a thermocouple for calibration. As shown in Section 4.2, the derived temperature from acetone vapor/air mixture was influenced by the laser energy and acetone concentration. The acetone mole fraction varied from 0.005 to 0.012, but the corresponding change in derived temperature was less than 4 K. Therefore, the influence on laser power and acetone concentration could be considered small, and the grating spacing calibration was performed for the acetone mole fraction of 0.012, as the acquired LITGS signal was best at this acetone mole fraction. By using the measured temperature at the LITGS measurement point and acquired oscillation frequency, the actual grating spacing was determined from Eq. (3) as 25.3±1 μm depending on the LITGS alignment. The focal length calculated from the measured grating spacing and the crossing angle calculated from the measured value were 894±4 mm and 0.64±0.02°, respectively.

The closed circle symbols in Fig. 5 represent the LITGS temperature calculated using the value of the calibrated grating spacing above rather than the originally assumed value. The revised temperatures are closer to the simulated values, especially at P = 0.3 MPa. In the case at P = 1.0 MPa, however, the derived temperatures were lower than that of the value of CHEMKIN simulations.

294

295 **4.2. Correction for laser light heating**

296 There is a tradeoff in obtaining robust LITGS signals by using high pulse energy, and the
297 generation of a local disturbance to the local temperature and density because LITGS is an absorption
298 based technique. A previous study [12] showed that the derived temperature from LITGS in acetone
299 or toluene increased linearly with an increase in concentration of absorbing media times laser energy.
300 Therefore, the influence of absorption should be considered when the incident laser energy and/or
301 concentration of absorbing media are sufficiently high. The total energy absorbed by the gas per unit
302 area, ΔE within a probe volume of length L, can be estimated by the Beer-Lambert Law as [24],

303 $$\Delta E = E_0\left\{1-\exp\left(-\sigma N_A n_{\mathrm{OH}} L\right)\right\} \approx E_0 \sigma N_A n_{\mathrm{OH}} L, \tag{4}$$

304 where σ, N_A, n_{OH} and E_0 are the absorption cross section, Avogadro's constant, the molar concentration
305 of OH and the total energy deposited, respectively. In the case where absorption is low, the exponential
306 term can be expanded, resulting in a linear behavior with the concentration of the absorbing species
307 and the initial energy. Considering that the probe volume heat capacity is mc_p (m: mass, c_p: mixture
308 averaged specific heat at constant pressure), the relative temperature rise by absorption of the incident
309 laser, ΔT, can be formulated as

310 $$\frac{\Delta T}{T_0} \propto \frac{\Delta E}{mc_p T_0} = \frac{E_0}{c_p T_0} \cdot \frac{\sigma N_A L}{VW} \cdot \frac{n_{\mathrm{OH}}}{n} \propto X_{\mathrm{OH}} E_0, \tag{5}$$

311 where V, n, X_{OH} are the probe volume, the molar density of mixture and the mole fraction of OH,
312 respectively.

313 We can therefore obtain the original temperature with no laser absorption by obtaining
314 measurements with different energies, and extrapolating the obtained LITGS frequency to the limit of
315 $E_0 \to 0$.

316 Figure 6 shows the relationship between derived temperature and pump energy at P = 0.5 MPa,
317 β = 0.6 and ϕ = 1.0. As shown in Fig. 6, the derived temperature increases linearly with an increase in
318 incident laser energy. By applying the linear extrapolation, the derived temperature with no

temperature rise can be determined as the intercept value of longitudinal axis. The *measured* resulting temperature slope for the condition where $P = 0.5$ MPa, $\beta = 0.6$ and $\phi = 1.0$ was 34.0 K/mJ. This large sensitivity arises because of the highly focused beam used to enhance signal and improve spatial resolution.

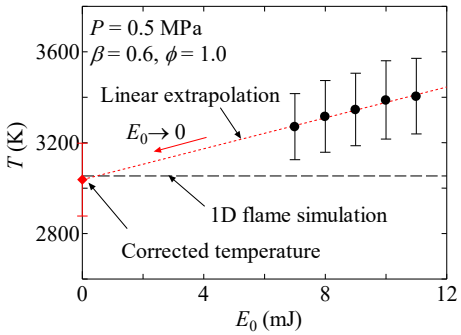

Figure 6. Relationship between apparent measured temperature, T, and pump laser energy, E_0.

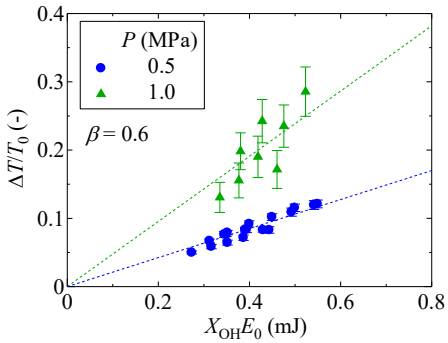

Figure 7. Relationship between normalized temperature rise by incident laser absorption, $\Delta T/T_0$, and the product $X_{OH}E_0$.

Although ideally this should be done for all cases, only a few conditions were evaluated over a range of energies. In the case for $P = 0.3$ MPa, the LITGS signal was relatively weak and it was not possible to draw an appropriate curve. Figure 7 shows the general relationship between normalized temperature rise, $\Delta T/T_0$, and the product of mole fraction of OH and incident laser energy, $X_{OH}E_0$, for a range of energies and mole fractions. Here, all examined equivalence ratio cases that the incident

laser power varied (i.e., ϕ = 0.6, 0.8, 1.0, 1.2 at P = 0.5 MPa; ϕ = 0.7 and 0.8 at P = 1.0 MPa) were plotted. The value of T_0 was determined from the extrapolation of the relationship between T and E_0. The temperature rise is also influenced by the molecular composition at the measurement point [12] which in turn depends on the operating condition. However, as shown in Fig. 7, the variation of $\Delta T/T_0$ with E_0 is linear in the range of energies considered, as expected from Eq. (5). The pressure effect is cancelled in Eq. (5) but the slope of $\Delta T/T_0$ depends on pressure as shown in Fig. 7. Here we only discuss the influence on incident laser energy and mole fraction of the absorbing species, but the rate of thermalization via collisions can also affect the derived temperature [13].

In the case at P = 0.5 MPa, the derived temperature agrees within 1.6% of the calculated adiabatic non-strained flame temperature (Fig. 5), with a calculated standard deviation of about 160 K at P = 0.5 MPa. We conclude that the temperature correction procedure must be systematically performed for accurate temperature evaluation. In the case at P = 1.0 MPa, the corrected temperatures appear to be lower than the calculated adiabatic values but the derived temperature is close to the temperature at 0.1 MPa obtained by OH-PLIF [21], suggesting that this may be the true value, and loss mechanisms may account for the discrepancy.

5. Conclusions

The study has demonstrated that LITGS temperatures can be successfully obtained using OH as the absorber in oxygen-enriched $CH_4/O_2/N_2$ flames up to 1.0 MPa and CH_4/O_2 flames at 0.3 MPa. The burned gas temperature can be derived from the LITGS signal, even for the mixtures where the flame temperature is as high as 3000 K. Therefore, the technique holds good potential for LITGS measurements under high pressure and high temperature flames, such as rocket combustion. Accurate measurements of temperature require calibration of the grating spacing, and correction for the temperature rise due to species absorption at high products of concentration and laser fluence. A procedure for temperature correction based on the linear extrapolation to zero absorption is recommended to minimize uncertainties.

Acknowledgement

This research was supported by the Collaborative Research Project of Institute of Fluid Science, Tohoku University (Project codes: J16089 and J17I026), the Mazda Foundation and the Grant-in-Aid for Young Scientists (A) (Project code: 17H04906). SL was supported by a DTA from EPSRC in the UK and grant EP/K02924X/1. The authors would like to thank F. De Domenico, University of Cambridge, for the useful comments, and P. Ewart and B. Williams of University of Oxford for their initial help with the LITGS.

References

[1] W. Mayer, H. Tamura, J. Propulsion Power 12 (1996) 1137-1147.

[2] K. Takeuchi, Y. Nunome, S. Tomioka, T. Tomita, T. Kudo, A. Hayakawa, H. Kobayashi, Trans. Jpn. Soc. Aeronautical Space Sci. 60 (2017) 116-123.

[3] Z. Xu, X. Tian, H. Zhao, Proc. Combust. Inst. 36 (2017) 4443-4451.

[4] F.T.C. Yuen, Ö.L. Gülder, Proc. Combust. Inst. 32 (2009) 1747-1754.

[5] C.N. Dennis, C.D. Slabaugh, I.G. Boxx, W. Meier, R.O. Lucht, Combust. Flame 173 (2016) 441-453.

[6] A. Stampanoni-Panariello, B. Hemmerling, W. Hubschmid, Appl. Phys. B 67 (1998) 125-130.

[7] J. Kiefer, P. Ewart, Prog. Energy Combust. Sci. 37 (2011) 525-564.

[8] R. Stevens, P. Ewart, Appl. Phys. B 78 (2004) 111-117.

[9] T. Seeger, J. Kiefer, M.C. Weikl, A. Leipertz, D.N. Kozlov, Opt. Express 14 (2006) 12994.

[10] B. Roshani, A. Flügel, I. Schmitz, D.N. Kozlov, T. Seeger, L. Zigan, J. Kiefer, A. Leipertz, J. Raman Spectrosc. 44 (2013) 1356-1362.

[11] B. Williams, M. Edwards, R. Stone, J. Williams, P. Ewart, Combust. Flame 161 (2014) 270-279.

[12] A. Hayakawa, S. Lowe, Y. Gao, L. Fan, S. Hochgreb, Proc. 16th Int. Symp. Adv. Fluid Inf. 16 (2016) 182-183.

[13] A.-L. Sahlberg, J. Kiefer, M. Aldén, Z. Li, Appl. Spectrosc. 70 (2016) 1034-1043.

[14] S. Williams, L.A. Rahn, P.H. Paul, J.W. Forsman, R.N. Zare, Opt. Lett. 21 (1994) 1681-1683.

[15] P.H. Paul, R.L. Farrow, P.M. Danehy, J. Opt. Soc. Am. B 12 (1995) 384-392.

[16] H. Latzel, A. Dreizler, T. Dreier, J. Heinze, M. Dillmann, W. Stricker, G.M. Lloyd, P. Ewart, Appl. Phys. B 67 (1998) 667-673.

[17] B. Hemmerling, D.N. Kozlov, Appl. Opt. 38 (1999) 1001-1007.

[18] A.-L. Sahlberg, D. Hot, J. Kiefer, M. Aldén, Z. Li, Proc. Combust. Inst. 36 (2017) 4515-4523.

[19] A. Luers, A.-L. Sahlberg, S. Hochgreb, P. Ewart, Appl. Phys. B 124 (2018) 43.

[20] H. Kobayashi, T. Tamura, K. Maruta, T. Niioka, F.A. Williams, Proc. Combust. Inst. 26 (1996)

389-396.

[21] K. Takeuchi, Y. Nunome, S. Tomioka, T. Tomita, T. Kudo, A. Hayakawa, H. Kobayashi, J. Therm. Sci. Technol. 13 (2018) JTST0001.

[22] ANSYS, CHEMKIN-PRO, 2016

[23] G.P. Smith, D.M. Golden, M. Frenklach, N.W. Moriarty, B. Eiteneer, M. Goldenberg, C.T. Bowmam, R.K. Hanson, S. Song, J. Garliner, C. William, V.V. Lissianski, Q. Zhiwei, GRI-MECH 3.0, available from http://www.me.berkeley.edu/gri_mech (2000).

[24] J.D. Koch, J. Gronki, R.K. Hanson, J. Quant. Spectros. Radiat. Transfer. 109 (2008) 2037-2044.

Figure captions

Fig. 1 Experimental setup and the layout of the optical geometry through the high pressure chamber for high pressure OH-LITGS experiments. The symbols M, BS, BD, F and PMT represent mirror, beam splitter, beam dump, interference filter and photo multiplier tube, respectively.

Fig. 2 Schematic figures of the modified burner nozzle for the calibration burner developed by Takeuchi et al. [21]: (a) Top-view; (b) Cross-sectional-view.

Fig. 3 (a) Flame image of direct photo and (b) instantaneous OH-PLIF image at P = 1.0 MPa for ϕ = 1.0 and β = 0.6.

Fig. 4 Representative single shot LITGS signal for the equivalence ratio of ϕ = 0.6: (a) P = 0.3 MPa, β = 0.6; (b) P = 0.3 MPa, β = 1.0; (c) P = 0.5 MPa, β = 0.6; (d) P = 1.0 MPa, β = 0.6.

Fig. 5 Derived temperature from the LITGS signals with and without corrections (see text): (a) P = 0.3 MPa, β = 0.6; (b) P = 0.3 MPa, β = 1.0; (c) P = 0.5 MPa, β = 0.6; (d) P = 1.0 MPa, β = 0.6. Solid lines are obtained from unstrained flame simulations.

Fig. 6 Relationship between apparent measured temperature, T, and pump laser energy, E_0.

Fig. 7 Relationship between normalized temperature rise by incident laser absorption, $\Delta T/T_0$, and the product $X_{OH}E_0$.